Thin Solid Films 552 (2014) 56–61

Contents lists available at ScienceDirect

Thin Solid Films

journal homepage: www.elsevier.com/locate/tsf

Effect of crystalline polarity on microstructure and optoelectronic properties of gallium-doped zinc oxide films deposited onto glass substrates

Tsuyoshi Ogino [a,b,c], Jesse R. Williams [a], Ken Watanabe [a], Isao Sakaguchi [a,c], Shunichi Hishita [a], Hajime Haneda [a,c], Yutaka Adachi [a], Takeshi Ohgaki [a,*], Naoki Ohashi [a,c]

[a] National Institute for Materials Science (NIMS), 1-1 Namiki, Tsukuba, Ibaraki 305-0044, Japan
[b] Research and Development Center, Taiyo Yuden Co., Ltd. 5607-2, Nakamuroda, Takasaki, Gunma 370-3347, Japan
[c] Department of Applied Science for Electronics and Materials (ASEM), Interdisciplinary Graduate School of Engineering Sciences, Kyushu University, 6-1 Kasugakoen, Kasuga, Fukuoka 816-8580, Japan

ARTICLE INFO

Article history:
Received 13 March 2013
Received in revised form 11 November 2013
Accepted 11 December 2013
Available online 18 December 2013

Keywords:
Zinc oxide film
Grain growth
Polarity
Doping

ABSTRACT

The effect of crystalline polarity on the microstructure of gallium-doped zinc oxide (GZO) deposited using magnetron sputtering onto glass substrates was investigated. X-ray photoelectron spectroscopy was used to determine the crystalline polarity of *c*-axis textured GZO films. Grains whose radii were more than 1 μm grew abnormally in 0.2 mol% doped GZO when the film was thicker than ~1 μm, and the radius of the grains was much smaller than 100 nm in the heavily (i.e., 4 mol%) doped GZO, regardless of the film thickness. Such abnormal growth of the grains in the 0.2 mol% doped GZO films coincided with a change in the crystalline polarity: the surfaces of unusually large GZO grains were terminated with the $(000\bar{1})$ face, and those of normal GZO grains were terminated with the (0001) face. The results indicated that polarity flipping is a very important event for controlling the texture of doped zinc oxide films.

1. Introduction

Electrodes produced with transparent thin films, including zinc oxide (ZnO) thin films, are one of the key technologies used to fabricate energy saving/harvesting devices [1–3]. Electrodes used for collecting electric charge require low resistance and high transparency in order to be used in high-efficiency photovoltaic cells [1]. Low energy loss in transparent electrodes is also important for low-energy operation of information displays and light-emitting diodes [2]. Further, transparent conductors are important in developing advanced windows for buildings and houses [3]. Toward that goal, several studies have been conducted on ZnO to develop transparent and conductive ZnO-based conductor films [4]. Significant attention has been paid to controlling charge compensation in ZnO in order to increase doping efficiency and decrease optical absorption owing to defects. When we consider the application of transparent electrodes to display devices such as liquid crystal displays and organic electroluminescence displays, transparent conductor films require very flat, smooth surfaces in order to prevent light scattering and inhomogeneity in the distribution of electric potential. However, transparent electrodes must show particular microstructural features such as grains that show large surface areas so that the transparent electrodes can be used in other applications such as dye-sensitized solar cells [5,6].

Group III impurities doped into ZnO films are widely known as effective donors [7]. There are many more reports to date about Al-doped ZnO films than there are about Ga- and In-doped ones. Most of the Al-doped ZnO films grown for application as transparent electrodes have been sputtered onto a-SiO_2 substrates, and the dependence of their electrical and optical properties including film-surface-texture-induced light scattering on growth conditions such as dopant concentration and film thickness has been investigated [8–10]. Numerous previous studies have focused on the microstructure and electrical properties of ZnO films [6,11,12]. Among the various ZnO films, the "milky white" ones have attracted our interest [12]. It has previously been indicated that milky white ZnO films are appropriate materials for application to the bottom electrodes in solar cells because of the light-scattering properties of the films. Milky white ZnO films have conventionally been prepared using direct current (DC) sputtering, and the preparation procedure is not very specific. Namely, it is uncommon for sputtering to result in irregularly textured films, and the mechanism underlying the formation of the film texture responsible for the milky whiteness is uncertain. In contrast, ZnO films prepared using chemical synthesis routes including hydrothermal [6] and solution deposition [11] often show some irregular or porous structures such as nanoflowers, so it is difficult to use chemical synthesis in order to deposit smooth continuous films. Obtaining chemically deposited ZnO

* Corresponding author. Tel.: +81 29 860 4665; fax: +81 29 855 1196.
E-mail address: OGAKI.Takeshi@nims.go.jp (T. Ohgaki).

0040-6090/$ – see front matter © 2013 Elsevier B.V. All rights reserved.
http://dx.doi.org/10.1016/j.tsf.2013.12.017

films showing high conductivity is difficult because of the gaps that naturally form between grains [11]. It is unlikely that a proper method of depositing ZnO films that show both high surface area and conductivity has been developed, so we are motivated to develop such a method. We used secondary ion mass spectroscopy with a very fine primary beam (NanoSIMS) [13] to distribute impurities in the textured films.

Here, we must also introduce a crystallographic feature of ZnO because its crystalline polarity affects many aspects of its properties. ZnO crystallizes in the wurtzite structure, which is a polar structure that consists of alternating stacks of cation and anion layers along its *c*-axis. Consequently, one c-face is the zinc (Zn)-terminated (0001) face and the other is the oxygen (O)-terminated $(000\bar{1})$ one. For example, the concentration of defects in a ZnO crystal depends on the crystalline sector of the dopant [14–16]. Indeed, donor impurities tend to incorporate into the $(000\bar{1})$ sector whereas acceptor impurities tend to incorporate into the (0001) one. We recently found that doping affects the crystalline polarity of ZnO thin films deposited using pulsed laser deposition (PLD) [17,18]. In fact, undoped PLD-grown ZnO films grown on sapphire (α-Al_2O_3) and silica glass (a-SiO_2) substrates showed an O-terminated $(000\bar{1})$ face, and heavily Al-doped ones grown on the same substrates showed a Zn-terminated (0001) one. Changes in the surface morphology of the films have also been associated with the direction of crystal growth. For example, ZnO films homoepitaxially deposited onto the (0001) and $(000\bar{1})$ faces of substrates show different surface morphologies [19].

Crystalline polarity is a very important aspect of both the microstructure and doping of ZnO thin films; thus, an appropriate method of determining polarity must be developed before the effects of crystalline polarity can be fully understood. There are several methods of determining the polarity of wurtzite structures [20–22]. We recently used X-ray photoelectron spectroscopy (XPS) to demonstrate how polarity is determined. Indeed, X-ray photoelectron diffraction (XPD) measurement [23] of the angle-dependent core-level peak intensity is an established method of determining polarity, and measuring valence band spectra at a normal emission geometry to observe the polarity-dependent valence band profile [18,24] is another appropriate method of determining polarity. In fact, the polarities of the polycrystalline ZnO films that show in-plane rotation domains (i.e., ZnO films deposited onto a-SiO_2 substrates) have previously been determined using the valence band [18] and XPD measurements [25].

In this paper, we report the microstructure and electronic properties of Ga-doped ZnO (GZO) thin films deposited using radiofrequency (RF) magnetron sputtering. We have reproduced the texture associated with milky white GZO and analyzed the properties of the films. We found that the change in the film microstructure correlated with the fluctuation in the concentration of Ga in the films.

2. Experiments

Most of the GZO films were deposited onto a-SiO_2 substrates, and some were deposited onto ZnO single-crystal substrates. All the substrates had very flat surfaces. We examined the (0001) and $(000\bar{1})$ faces of the ZnO substrates to determine what effect the crystalline polarity of the substrate had on the microstructure of the deposited films. The GZO films were deposited using RF magnetron sputtering with a commercial deposition system. The pressure in the chamber was maintained at 1–2 Pa by balancing pumping with the flow of argon gas. The typical RF electric power loaded to the magnetron head was 150 W. The targets were 3-inch-diameter polycrystalline 0.2 and 4 mol% (molar fraction of Ga/(Ga + Zn)) Ga-doped GZO ceramics prepared using ordinary sintering. A target was fixed ~40 mm below the substrate. The GZO films were sputtered at 30 nm/min for 5–100 min. The substrates were heated in the range 50–150 °C during deposition because they were exposed to the plasma. Hereafter, the 0.2 and 4 mol% Ga-doped GZO are abbreviated as GZO-0.2 and GZO-4.0.

The microstructures of the obtained films were characterized using X-ray diffraction (XRD, PANalytical X'Pert Pro MRD equipped with a hybrid 2-bounce asymmetric Ge (220) monochromator and a Cu Kα radiation source) and scanning electron microscopy (SEM, Carl Zeiss SUPRA 35VP, operation voltage = 7 kV). The distributions of the dopants in the films were analyzed using two secondary ion mass spectroscopy (SIMS) systems: a CAMECA IMS 4f and a CAMECA NanoSIMS-50 spectrometer. $^{133}Cs^+$, whose ion energy was 8 kV, was tuned on the sample surface, and $(^{64}Zn + {}^{16}O)^-$ and $(^{71}Ga + {}^{16}O)^-$ molecular ions were collected using a multicollection system. The crystalline polarity of the films; i.e., whether the surface was a Zn-terminated (0001) or an O-terminated $(000\bar{1})$ face, was determined using XPS measured with normal emission geometry [24]. A Σ-probe spectrometer (Thermo Fisher Scientific, K.K., equipped with a monochromated Al Kα radiation source (beam energy: 1486 eV) and a sample goniometer) was used for the XPS measurements. The sample surfaces were sputtered using Ar gas before the measurements. The C 1s peak in each spectrum was applied to correct the binding-energy reference. The optical properties of the GZO films were evaluated using regular transmittance measurements (JASCO Corp. V-550) in the range $\lambda = 300$–900 nm at room temperature. The electric resistivity (ρ) of the GZO films was measured using the DC four-probe method in which the electrodes were configured in the van der Pauw geometry. Hall measurements (Toyo Corp., ResiTest 8300) were also performed to evaluate the concentration of electrons (n_e) and the Hall carrier mobility (μ_e) of the resultant films. The ohmic electrodes used for the electrical measurements were produced by evaporating indium metal under vacuum.

3. Results and discussion

XRD θ–2θ patterns typical of the GZO-0.2 and GZO-4.0 films grown on the a-SiO_2 substrates are shown in Fig. 1. The θ–2θ patterns only show the diffraction peaks assignable to the (0002) and (0004) planes, indicating that the obtained films are well-aligned *c*-axis-oriented ones.

Fig. 2 shows the electric transport properties of the GZO-4.0 films deposited in various thicknesses onto a-SiO_2 substrates. The electric transport properties are plotted as functions of film thickness. The ZnO films often showed decreasing ρ with increasing thickness [7,26]. Although n_e was close to the concentration of Ga atoms in the 4 mol% Ga-doped ZnO target (1.8×10^{21} cm^{-3}) regardless of the film thickness, μ_e increased with increasing thickness. Thus, the decreased conductivity of the thinner films is attributed to the low crystallinity of the films during nucleation. The GZO-0.2 films showed a similar trend: n_e for the GZO-0.2 films was one order of magnitude less than

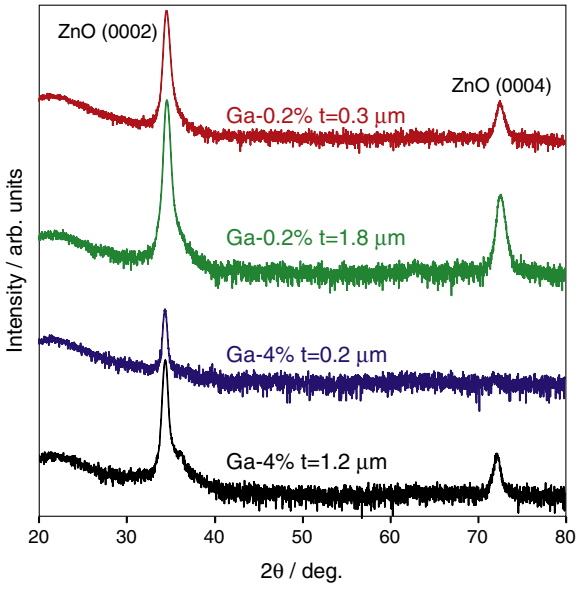

Fig. 1. XRD patterns for Ga-doped ZnO films grown on a-SiO_2 substrates.

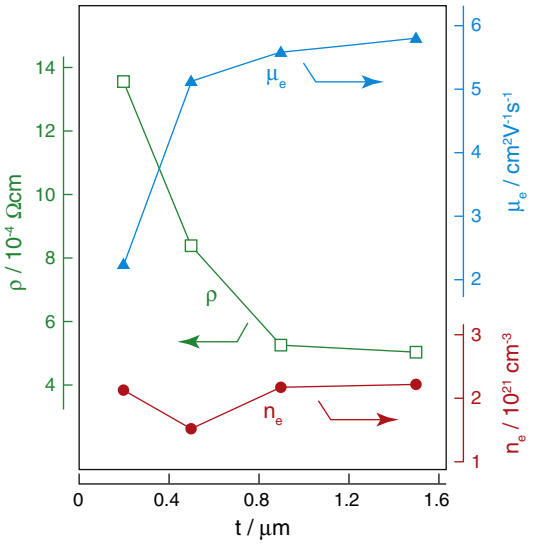

Fig. 2. Electric resistivity (ρ), electron concentration (n_e), and electron mobility (μ_e) plotted as functions of film thickness for 4 mol% Ga-doped ZnO films deposited onto a-SiO_2 substrates.

that for the GZO-4.0 films because of the lower concentration of Ga in the GZO-0.2 films. The thicker films clearly show better electrical conductivity than the thinner ones.

However, increasing the thickness of the films is not always a good idea for producing transparent conductor films. Fig. 3 shows the optical transmittance spectra for the films deposited in various thicknesses onto a-SiO_2 substrates. The transmittance of the films decreased with increasing film thickness. In particular, the transmittance of the GZO-0.2 film was obviously lower when the film was thicker than 1 μm, as shown in Fig. 3(a). The GZO-0.2 film thicker than 1 μm appeared milky white to the naked eye. In contrast to the GZO-0.2 films, the GZO-4.0 ones showed relatively high transparency even when the film was thicker than 1.5 μm, as shown in Fig. 3(b). The transmittance in the infrared (IR) range for the GZO-4.0 films was lower than that for the GZO-0.2 ones, and the blue-shift in the absorption edge was more significant for the GZO-4.0 films than for the GZO-0.2 ones. The blue-shift was caused by electrons filling into the conduction band as a result of a high concentration of donors [27,28]. These optical characteristics of the GZO films produced with higher Ga concentrations were due to the higher n_e achieved through heavy doping. Fig. 4 shows the average transmittance in the visible range of the spectrum plotted as functions of film thickness. The GZO-0.2 film clearly shows a steeper decrease in transmittance than the GZO-4.0 one does with increasing film thickness.

The SEM images shown in Fig. 4 explain why the optical transmittance of the GZO-0.2 films decreased with increasing thickness. The unusually large grains in the GZO-0.2 films most probably scattered the visible light thereby degrading the regular transmittance of the films because the density and diameter of the unusually large grains both increased with increasing film thickness. In fact, many larger grains started appearing when the film was ~350 nm thick (see SEM image A), and the density and radius of those large grains both increased with increasing film thickness (see SEM image B). The surface of the GZO-0.2 film was completely covered with such larger grains when the film was thicker than 1 μm. In contrast, the average diameter of the grains in the GZO-4.0 films thicker than 1 μm, shown in images C and D in Fig. 4, was still on the order of 10 nm. The regular transmittance spectra shown in Fig. 3 is influenced by scattering. Therefore, it is reasonable that the decreased regular transmittance of the thick GZO-0.2 film was attributed to the growth of unusually large grains and to light scattering caused by them.

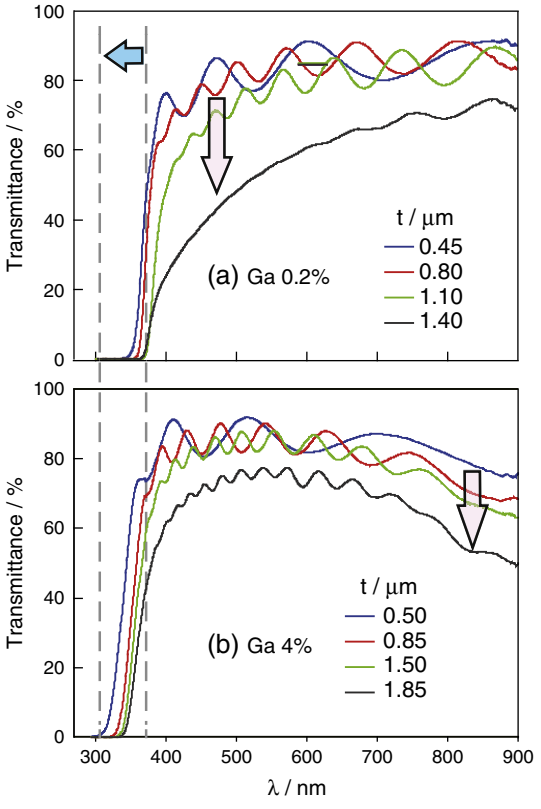

Fig. 3. Regular transmittance spectra for (a) 0.2 and (b) 4 mol% Ga-doped ZnO films produced with various thicknesses.

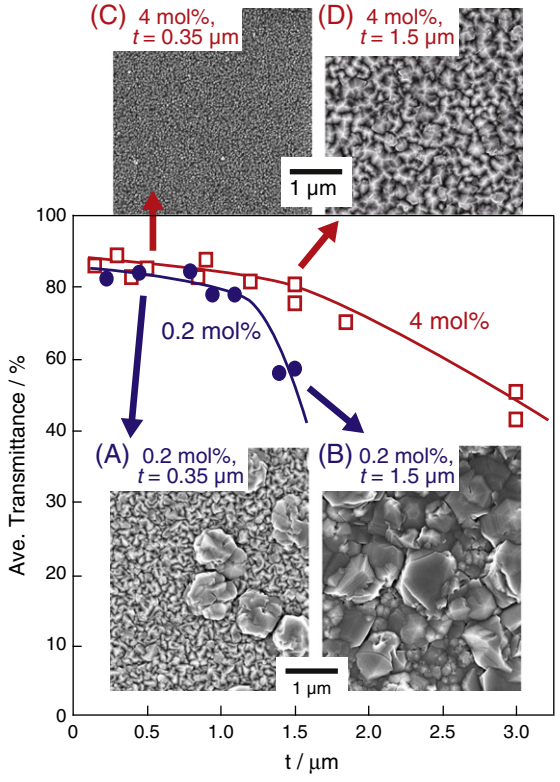

Fig. 4. Average transmittance in visible-light range plotted as functions of film thickness for 0.2 and 4 mol% Ga-doped ZnO films produced with various thicknesses. Insets show scanning electron microscopy images of 0.35- and 1.5-μm-thick (a and b) 0.2 and (c and d) 4 mol% Ga-doped ZnO films.

The Ga-concentration mapping performed using NanoSIMS indicated that the GZO-0.2 film deposited onto the a-SiO_2 substrate was not uniform, as shown in Fig. 5(a). The film in this mapping image shows sparsely distributed large grains, similar to those shown in image A in Fig. 4. The line scan profile for the relative Ga concentration and a schematic drawing of the film structure are shown in Fig. 5(b). The GZO-4.0 film did not show such nonuniformity within the spatial resolution of NanoSIMS. Although the NanoSIMS probe size was absolutely too large (ca. 50 nm) to resolve the small grains in the GZO-4.0 film, the concentration of Ga in the GZO-4.0 film was very homogeneous within the NanoSIMS resolution.

A previous study on DC-sputtered ZnO films doped with a relatively low concentration (0.75%) of Ga reported similar abnormal grain growth [12]. Grain growth is commonly inhibited in heavily (>1 mol%) doped ZnO not only in films deposited using sputtering onto a-SiO_2 substrates [12,29] but also in those deposited using PLD and those deposited onto single-crystalline wafers; e.g., sapphire substrates [18]. The relation between the concentration of dopant and the size of the grains in Al-doped ZnO films was previously reported [8,9]. According to these reports, grain size clearly increased with decreasing concentration of Al dopant in the films. Thus, it is likely that only ZnO films doped with relatively low concentrations of Ga show abnormal grain growth. Considering the fluctuation in the composition of the GZO-0.2 films, we hypothesized that the solubility limit of Ga in ZnO (Δ_{Ga}^{ZnO}) is an important parameter for understanding the phenomena observed in this study. Δ_{Ga}^{ZnO} increases with increasing temperature at equilibrium and is in the range 0.25–0.4 mol% ($\leq 10^{19}$ cm^{-3}) after sufficient thermal relaxation in the range 800–1000 °C [30,31]. Namely, films containing concentrations of Ga above Δ_{Ga}^{ZnO} consist of a metastable phase. The concentration of Ga in the GZO-0.2 films was close to Δ_{Ga}^{ZnO}; thus, spatial fluctuation in the concentration of Ga may have induced the coexistence of metastable ZnO grains whose concentration of Ga exceeded Δ_{Ga}^{ZnO} and stable ones whose concentration of Ga was below or the same as Δ_{Ga}^{ZnO}.

Fig. 6 shows XPS spectra for the films produced at various thicknesses and concentrations of dopant. The peaks in the valence band spectra for the GZO-4.0 films (i.e., spectra C and D) were broader and had shifted to higher binding energies than those in the valence band spectra for bulk ZnO (i.e., spectra A and B). Such broadening and shifting were due to doping. Doping ZnO with Ga atoms causes additional deep states in the valence band. The valence band spectra include information about the crystalline polarity of ZnO, as mentioned in the Introduction. In fact, the spectrum for the (0001) face of bulk ZnO single crystal showed a subpeak at ~4.5-eV binding energy (see spectrum A), appropriate for identifying the polarity of the film [18,24], but that for the $(000\bar{1})$ face of bulk ZnO single crystal did not (see spectrum B). The spectra for the thick (1.2-μm-thick) and thin (250-nm-thick) GZO-4.0 films (i.e., spectra C and D, respectively) showed the subpeak, indicating a (0001) face on top of the GZO-4.0 films regardless of the film thickness. The tendency for the (0001) face to be on top of the GZO-4.0 films because of heavy doping with donor impurities is true not only when the films are deposited onto a-SiO_2 substrates but also when various substrates and deposition methods are used. For instance, PLD-deposited ZnO films have also shown (0001)-terminated ZnO due to heavy Al-doping, as reported elsewhere in the literature [17,18].

In contrast to the valence band profile for the GZO-4.0 films, that for the GZO-0.2 ones varied with film thickness. The valence band spectrum for the relatively thin film (i.e., spectrum E) was similar to that for the

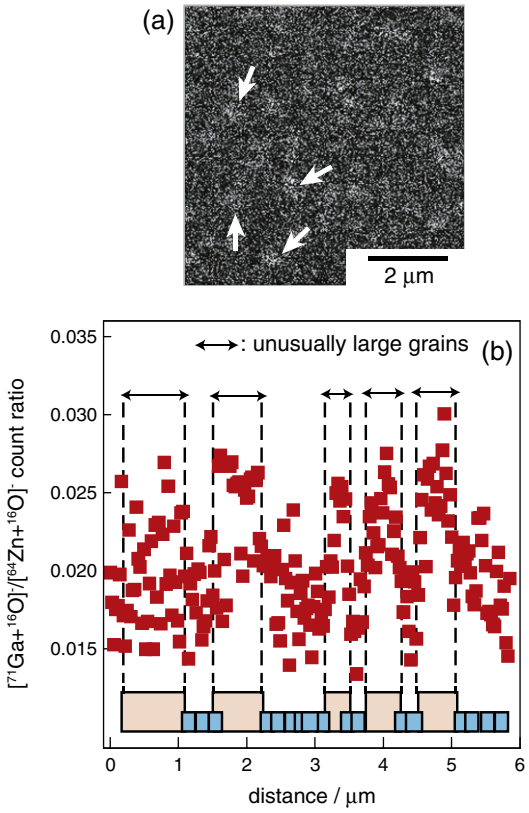

Fig. 5. SIMS analyses of Ga concentration in 0.2 mol% Ga-doped ZnO films. (a) Concentration mapping for thin (i.e., 0.3-μm-thick) film and (b) typical line profile for thick (i.e., 1.8-μm-thick) film showing schematic film structure. Arrows in panel a indicate unusually large grains in films, and double-headed arrows in panel b indicate regions of unusually large grains in line profile.

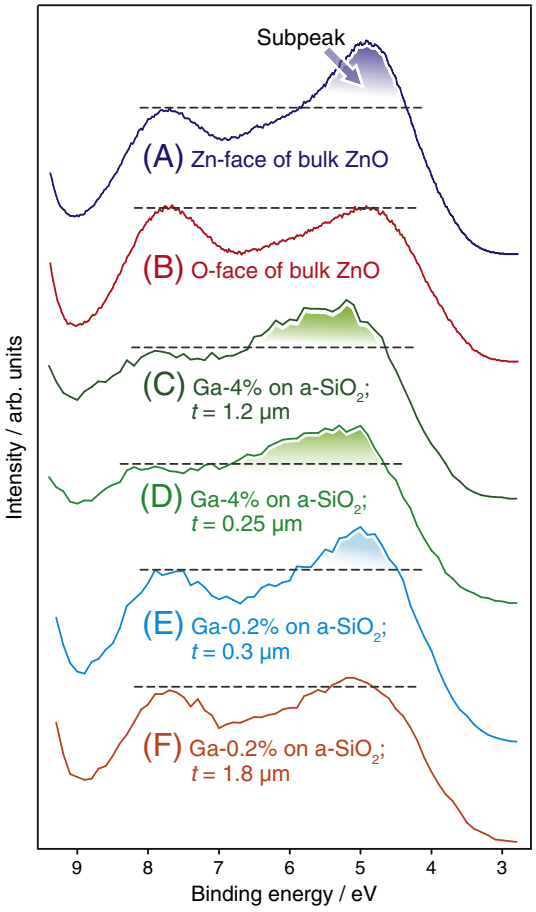

Fig. 6. XPS spectra for 0.2 mol% Ga-doped ZnO films (e and f) and 4 mol% Ga-doped ZnO films (c and d) of various thicknesses deposited onto a-SiO_2 substrates. XPS spectra for (0001) and $(000\bar{1})$ faces of ZnO single crystal (a and b) are also shown for reference. Here, Zn- and O-face denote (0001) and $(000\bar{1})$ faces of ZnO single crystal, respectively.

Zn-face of bulk ZnO (i.e., spectrum A), and that for the relatively thick film (i.e., spectrum F) was similar to that for the O-face of bulk ZnO (i.e., spectrum B). These results indicated that the surface of the relatively thin (i.e., less than 300-nm-thick) GZO-0.2 film showed Zn-terminated (0001) faces and was composed of very fine grains. However, the surface of the GZO-0.2 film showed more O-terminated ($000\bar{1}$) faces with increasing film thickness, suggesting that although the nucleation of the GZO-0.2 films had been initiated by the formation of Zn-terminated grains, the large grains in the GZO-0.2 films showed O-terminated surfaces.

It is worth noting that the results obtained for the GZO-0.2 film deposited onto the ZnO single-crystal substrate were similar to those obtained for the same deposited onto the a-SiO_2 substrate. Indeed, the GZO-0.2 film deposited onto the ZnO substrate showed a very rough surface regardless of the crystalline polarity of ZnO substrate, and such microstructure resulted in decreased transparency of the film. Moreover, the GZO-0.2 films deposited onto ZnO single-crystal substrates also showed the change in polarity. Fig. 7 shows valence band spectra for the GZO-0.2 films deposited onto the ZnO single-crystal substrates. None of the profiles for the films (not even the one for the film deposited onto the (0001) face of the ZnO substrate) showed the subpeak, which is a fingerprint characteristic of the (0001) surface, when the valence band profiles for the films were compared with that for bulk single crystal. This means that the Ga-doped ZnO that showed the ($000\bar{1}$) face had been nucleated on the (0001) face of the ZnO single crystal.

Fig. 8 shows a summary of the experimental results. The GZO-0.2 films showed abnormal grain growth, an important cause of visible light scattering that decreased the optical transmittance of the films, while the GZO-4.0 films did not. Moreover, the crystalline polarity of the films simultaneously changed from the (0001) to the ($000\bar{1}$) face with the formation of large grains. Thus, it is plausible that the formation of the grains that were terminated with a ($000\bar{1}$) face triggered the abnormal grain growth, resulting in the formation of a very specific microstructure.

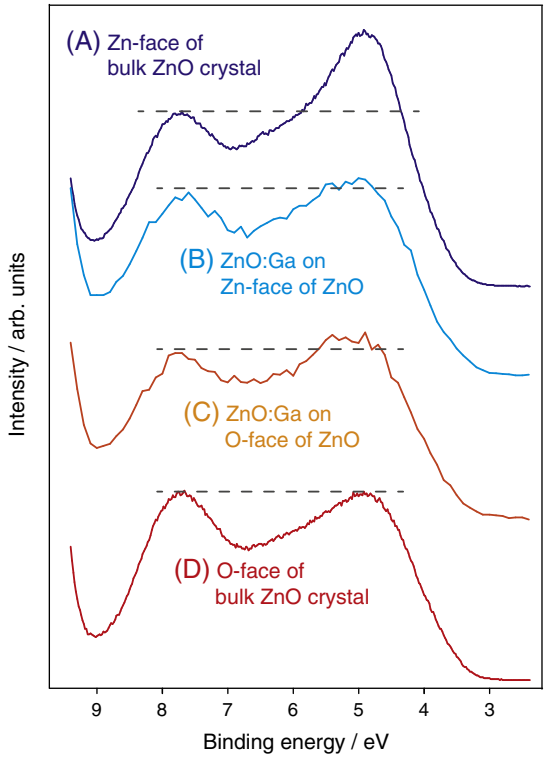

Fig. 7. XPS spectra for 0.2 mol% Ga-doped ZnO deposited onto ZnO single-crystal substrates (b and c) and those for single-crystal ZnO (a and d). Here, Zn- and O-face denote (0001) and ($000\bar{1}$) faces of ZnO single crystal, respectively.

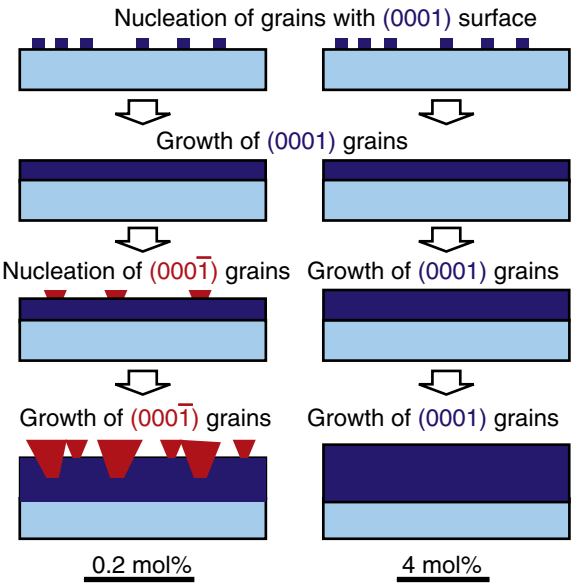

Fig. 8. Evolution of film morphology and change in crystalline polarity with increasing film thickness.

The possible reason for crystalline polarity flipping and unusually large grains in the GZO films is found in the inhomogeneous incorporation of impurities during ZnO crystal growth using a hydrothermal method. It has previously been indicated that the ($000\bar{1}$) facet attracts the incorporation of donors, and, in contrast, the (0001) facet attracts the incorporation of acceptors [14,15]. The concentrations of Ga in the unusually large grains were slightly higher than that of Ga in the small ones, and such large grains showed ($000\bar{1}$) surfaces. If the ($000\bar{1}$) facets attract the incorporation of donor impurities, even during sputtering deposition, a relatively high concentration of Ga in large grains terminated with a ($000\bar{1}$) face is consistent with the results obtained for the hydrothermally grown GZO films.

The true mechanism governing the behavior of grain growth in the GZO films cannot be completely understood based on the findings in this study. Although only the stabilization of the grains showing ($000\bar{1}$) surfaces in the slightly doped film was not well-explained, the spatial fluctuation in the concentration of Ga in the grains is most probably why they had formed. It is at least true that the crystalline polarity of ZnO grains is of great concern in controlling the formation of the microstructure in ZnO films. We propose that polarity analyses are necessary to reveal the formation of the microstructure in ZnO films and to understand the behavior of crystal growth.

4. Conclusions

GZO films were deposited using RF magnetron sputtering. Previously observed abnormal grain growth was reproduced in the film doped with a relatively low concentration of Ga. Very large grains started forming in the GZO-0.2 films thicker than a few hundred nanometers, and the surfaces of the GZO-0.2 films thicker than 1 μm were nearly completely covered with unusually large grains. The grains seemed to simultaneously begin growing abnormally with polarity flipping. The surfaces of the GZO-0.2 films were terminated with the ($000\bar{1}$) face after the grains in the films began growing abnormally. The heavily doped GZO films tended to show surfaces terminated with the (0001) face. Although the essential mechanism for the abnormal growth of the grains in the films is uncertain, we suppose that spatial fluctuations in the compositions of Ga in the grains may trigger the polarity flipping, forming unusually large grains.

Controlling the size of grains is crucial for improving the transparency of Ga-doped ZnO films. Thus, managing abnormal grain growth, which is associated with polarity flipping, should be a very important issue for applying ZnO-based transparent conductor films to a wide range of optoelectronic devices, and further studies are needed to understand the abnormal grain growth.

Acknowledgements

This study was partly supported by a Grant-In-Aid for Scientific Research (B) No. 22360277 from the Japan Society for the Promotion of Science (JSPS), Japan.

References

[1] M.M. Islama, S. Ishizuka, A. Yamada, K. Matsubara, S. Niki, T. Sakurai, K. Akimoto, Appl. Surf. Sci. 257 (2011) 4026.
[2] H. Yamauchi, M. Iizuka, K. Kudo, Jpn. J. Appl. Phys. 46 (2007) 2678.
[3] G. Walters, I.P. Parkin, Appl. Surf. Sci. 255 (2009) 6555.
[4] T. Minami, Semicond. Sci. Technol. 20 (2005) S35.
[5] T. Yoshida, H. Minoura, Adv. Mater. 12 (2000) 1219.
[6] C.Y. Jiang, W.W. Sun, G.Q. Lo, D.L. Kwong, J.X. Wang, Appl. Phys. Lett. 90 (2007) 263501.
[7] T. Minami, H. Sato, H. Nanto, S. Takata, Jpn. J. Appl. Phys. 24 (1985) L781.
[8] I. Sieber, N. Wanderka, I. Urban, I. Dörfel, E. Schierhorn, F. Fenske, W. Fuhs, Thin Solid Films 330 (1988) 108.
[9] N. Ehrmann, Development of selective coating systems for solar-thermal flat-plate collectors, (dissertation) University of Hannover, Germany, 2012.
[10] F. Fenske, B. Selle, M. Birkholz, Jpn. J. Appl. Phys. 44 (2005) L662.
[11] H. Wagata, N. Ohashi, K.-I. Katsumata, H. Segawa, Y. Wada, H. Yoshikawa, S. Ueda, K. Okada, N. Matsushita, J. Mater. Chem. 22 (2012) 20706.
[12] H. Sato, T. Minami, Y. Tamura, S. Tanaka, T. Mouri, N. Ogawa, Thin Solid Films 246 (1994) 86.
[13] I. Sakaguchi, K. Watanabe, S. Hishita, N. Ohashi, H. Haneda, Jpn. J. Appl. Phys. 51 (2012) 101801.
[14] N. Ohashi, T. Ohgaki, S. Sugimura, K. Maeda, I. Sakaguchi, H. Ryoken, I. Niikura, M. Sato, H. Haneda, Mater. Res. Soc. Symp. Proc. 799 (2004) Z5.
[15] H. Maki, I. Sakaguchi, N. Ohashi, S. Sekiguchi, H. Haneda, J. Tanaka, N. Ichinose, Jpn. J. Appl. Phys. 42 (2003) 75.
[16] E. Ohshima, H. Ogino, I. Niikura, K. Maeda, M. Sato, M. Ito, T. Fukuda, J. Cryst. Growth 260 (2004) 166.
[17] Y. Adachi, N. Ohashi, T. Ohnishi, T. Ohgaki, I. Sakaguchi, H. Haneda, M.J. Lippmaa, J. Mater. Res. 23 (2008) 3269.
[18] Y. Adachi, N. Ohashi, T. Ohgaki, T. Ohnishi, I. Sakaguchi, S. Ueda, H. Yoshikawa, K. Kobayashi, J.R. Williams, T. Ogino, H. Haneda, Thin Solid Films 519 (2011) 5875.
[19] H. Matsui, H. Saeki, T. Kawai, A. Sasaki, M. Yoshimoto, M. Tsubaki, H. Tabata, J. Vac. Sci. Technol. B 22 (2004) 2454.
[20] T. Ohnishi, A. Ohtomo, M. Kawasaki, K. Takahashi, M. Yoshimoto, H. Koinuma, Appl. Phys. Lett. 72 (1998) 824.
[21] T. Mitate, K. Sonoda, N. Kuwano, Phys. Status Solidi A 192 (2002) 383.
[22] H. Tampo, P. Fons, A. Yamada, K. Kim, Appl. Phys. Lett. 301–302 (2005) 358.
[23] J.R. Williams, M. Kobata, I. Pis, E. Ikenaga, T. Sugiyama, K. Kobayashi, N. Ohashi, Surf. Sci. 605 (2011) 1336.
[24] N. Ohashi, Y. Adachi, T. Ohsawa, K. Matsumoto, I. Sakaguchi, H. Haneda, S. Ueda, H. Yoshikawa, K. Kobayashi, Appl. Phys. Lett. 94 (2009) 122102.
[25] J.R. Williams, I. Pis, M. Kobata, A. Winkelmann, T. Matsushita, Y. Adachi, N. Ohashi, K. Kobayashi, J. Appl. Phys. 111 (2012) 033525.
[26] D. Dimova-Malinovska, N. Tzenov, M. Tzolov, L. Vassilev, Mater. Sci. Eng. B 52 (1998) 59.
[27] E. Burstein, Phys. Rev. 93 (1954) 632.
[28] T.S. Moss, Proc. Phys. Soc. Lond. B67 (1954) 775.
[29] K. Sivakumar, S.M. Rossnagel, J. Vac. Sci. Technol. A 28 (2010) 515.
[30] J. Kobayashi, N. Ohashi, H. Sekiwa, I. Sakaguchi, M. Miyamoto, Y. Wada, Y. Adachi, K. Matsumoto, H. Haneda, J. Cryst. Growth 311 (2009) 4408.
[31] T. Nakagawa, I. Sakaguchi, M. Uematsu, Y. Sato, N. Ohashi, H. Haneda, Y. Ikuhara, Jpn. J. Appl. Phys. 46 (2007) 4099.